Highly selective photocatalytic reduction of carbon dioxide with water over silver-loaded calcium titanate

AUTHOR(S):

Anzai, Akihiko; Fukuo, Naoto; Yamamoto, Akira; Yoshida, Hisao

Highly selective photocatalytic reduction of carbon dioxide with water over silver-loaded calcium titanate

Akihiko Anzai,[a] Naoto Fukuo,[a] Akira Yamamoto,[a,b] and Hisao Yoshida[a,b,*]

[a] *Kyoto University, Graduate School of Human and Environmental Studies, Kyoto 606-8501, Japan*

[b] *Kyoto University, Elements Strategy Initiative for Catalysts and Batteries (ESICB), Kyoto 615-8520, Japan*

*E-mail: yoshida.hisao.2a@kyoto-u.ac.jp

Abstract

The once reported Ag-modified $CaTiO_3$ photocatalyst was reexamined by optimizing the Ag loading amount and using a conventional photochemical reactor. This revealed that the Ag-modified $CaTiO_3$ photocatalyst actually showed both high production rate of CO (54 μmol h^{-1}) and excellent selectivity toward CO formation (94%) by suppressing the H_2 production via water splitting. It is suggested that the high photocatalytic performance originates from not only the optimized amount of cocatalyst and the high irradiation light intensity but also the high concentration of dissolved CO_2 that was achieved by a bubbling flow of CO_2 at the lower reaction temperature. These reaction conditions provided ca. 40 times higher CO formation rate. It was proposed that the deposited small Ag nanoparticles are the selective active sites for CO formation and the $CaTiO_3$ crystal surface produces H_2 preferably.

Keywords: Artificial photosynthesis; Reduction of carbon dioxide; Calcium titanate; Carbon monoxide.

1. Introduction

Heterogeneous photocatalytic reduction of CO_2 by using water has been widely studied as one of the possible ways to convert CO_2 to other beneficial chemicals such as CO, CH_3OH, CH_4, etc. by using solar energy [1–3], which is called as artificial photosynthesis [4–7]. Recently, various heterogeneous powder photocatalysts that can constantly produce CO, H_2 and O_2 with the stoichiometric ratio of the reductive and oxidative products have been reported [8–16], such as Cu-loaded ZrO_2 [8], Ag-loaded $ALa_4Ti_4O_{15}$ (A = Ca, Sr and Ba) [9], Ag-loaded $KCaSrTa_5O_{15}$ [10], Ag-loaded $La_2Ti_2O_7$ [11], and Ag-loaded $ZnTa_2O_6$ [12]. In these photocatalytic reaction systems, the reduction of CO_2 to CO (eq. 1) and the reduction of proton to hydrogen (eq. 2), and the oxidation of water to O_2 (eq. 3) are promoted simultaneously, and thus, the CO_2 decomposition to CO and O_2 (eq. 4) and the water decomposition to H_2 and O_2 (eq. 5) take place

competitively. From the equations 1 and 3, it is obvious that water is necessary for the CO_2 decomposition as an electron source in the oxidation part.

Since the redox potential for proton (0.0 V, vs. SHE) is higher than that for CO_2 to CO (−0.12 V, vs. SHE) [17], H_2 has always been observed as the competitive reductive products through water splitting. When no other reductive products than CO and H_2 are observed in these systems, the CO selectivity, S_{CO} (%), and the ratio of the consumed electron and hole, e^-/h^+, can be calculated according to the equations 6 and 7, respectively [14], where the production rate of CO, H_2 and O_2 are referred to as R_{CO}, R_{H2} and R_{O2}, respectively.

$$CO_2 + 2\,H^+ + 2\,e^- \rightarrow CO + H_2O \quad (1)$$

$$2\,H^+ + 2\,e^- \rightarrow H_2 \quad (2)$$

$$H_2O + 2\,h^+ \rightarrow 1/2\,O_2 + 2\,H^+ \quad (3)$$

$$CO_2 \rightarrow CO + 1/2\,O_2 \quad (4)$$

$$H_2O \rightarrow H_2 + 1/2\,O_2 \quad (5)$$

$$S_{CO}\,(\%) = 100 \times R_{CO} / (R_{CO} + R_{H2}) \quad (6)$$

$$e^-/h^+ = (\text{electrons consumed for } H_2 \text{ and CO formation}) / (\text{holes consumed for } O_2 \text{ formation}) = (R_{CO} + R_{H2}) / 2\,R_{O2} \quad (7)$$

Recently, several photocatalysts have been found to exhibit high CO selectivity, i.e., higher production rate of CO than that of H_2, for example, Ag-loaded $NaTaO_3$:Ba [13], Ag-loaded $Sr_2KTa_5O_{15}$ [14], and Ag-loaded, Zn-doped Ga_2O_3 [15,16]. Among them, especially, Ag/$ZnGa_2O_4$ recorded a very high CO selectivity such as 96 % [16]. In these studies, some reasons for the high CO selectivity has been proposed, e.g., the bubbling CO_2 in the presence of sodium bicarbonate ($NaHCO_3$) would increase the concentration of CO_2 as a reactant around the photocatalyst [13,14], and the number of the active sites for H_2 formation would be decreased by the loaded Ag cocatalyst [15] or the inactive surface layer such as $ZnGa_2O_4$ on Ga_2O_3 photocatalyst [16].

Calcium titanate has been studied as a photocatalyst for water splitting [18,19], photocatalytic steam reforming [19,20] and so on. The $CaTiO_3$ photocatalyst has a conduction band with a high potential enough to reduce both CO_2 and proton to produce CO and H_2, respectively [21]. Previously, we once reported that Ag-loaded $CaTiO_3$ polyhedral crystals can promote the photocatalytic reduction of CO_2 to produce CO and O_2 along with the water splitting to form H_2 and O_2 [22], where the CO selectivity was not so high such as

45% at the steady state [22]. In the present study, we examined the Ag-loaded $CaTiO_3$ photocatalyst by optimizing Ag-loading amount and changing the reactor. As a results, the original photocatalytic activity of the Ag-loaded $CaTiO_3$ photocatalyst was uncovered, i.e., the new reaction condition much improved the photocatalytic activity of the Ag-loaded $CaTiO_3$ photocatalyst for the CO_2 reduction, not only the CO production rate but also the CO selectivity, compared to those in the previous study [22].

2. Experimental

2.1. Catalyst preparation

$CaTiO_3$ sample was similarly prepared via a flux method [22] from $CaCO_3$ (Kojundo 99.99%) and TiO_2 (rutile, Kojundo 99.99%) as starting materials with NaCl (Kishida 99.5%) as a flux. The starting materials and the flux were physically mixed by a mortar, where the molar ratio of $CaCO_3$ to TiO_2 was 1:1 and that of the starting materials to the flux was 4:6. The mixed powder in an aluminum crucible was heated by an electric muffle furnace up to 1373 K at a rate of 200 K h^{-1}, held at this temperature for 10 h, cooled down to 773 K at a rate of 100 K h^{-1} and then naturally cooled down to room temperature. The resulting powder was washed four times with hot water (353 K, totally 2 L). Ag cocatalyst was loaded on the surface of the $CaTiO_3$ photocatalysts by a photodeposition method. The $CaTiO_3$ powder of 1.0 g was introduced to a quartz tube with 20 ml of aqueous $NaHCO_3$ solution (1.0 mol L^{-1}) and required amount of aqueous $AgNO_3$ solution. Bubbling with a helium gas, photoirradiation was carried out using a 300 W xenon lamp for 24 h, where the light intensity was measured to be 50 mW cm^{-2} at 365±20 nm in wavelength. The irradiation wavelength was limited to the range from 350 to 500 nm by using both a UV cold mirror and an ultraviolet-cut filter. The loading amount of Ag was confirmed by X-ray florescence analysis. The obtained samples were referred as to Ag(*x*)/$CaTiO_3$, where *x* means the loading amount of Ag cocatalyst in weight %.

2.2. Characterizations

Scanning electron microscopy (SEM) image was recorded by a JEOL JSM-890 in a secondary electron detection mode. Powder X-ray diffraction (XRD) pattern was recorded by a Shimadzu Lab X XRD-6000 with Cu Kα radiation (40 kV, 30 mA). Diffuse reflectance UV–Vis spectrum was recorded on a JASCO V-670 equipped with an integrating sphere covered with $BaSO_4$ as the reference.

2.3. Photocatalytic reduction of CO_2

Photocatalytic reaction test was carried out in a commercially obtained conventional inner irradiation photochemical reactor equipped with a 100 W high pressure mercury lamp, where the light intensity was

measured to be 44 mW cm^{-2} at 254±10 nm in wavelength (Table S1, Reactor B). The reaction temperature was 288 K. The irradiation area was 154.5 cm^2. The Ag(*x*)/$CaTiO_3$ photocatalyst powder of 0.3 g was dispersed in 360 mL of an aqueous $NaHCO_3$ solution (1.0 mol L^{-1}), where bicarbonate ion (HCO_3^-) derived from $NaHCO_3$ works as a buffer to enable the dissolution of much more CO_2 into the solution [23]. The photocatalyst was suspended with magnetically stirring in a bubbling flow of gaseous CO_2 at a flow rate of 30 mL min^{-1} for 4 h in the dark, and then the lamp was switched on to start the photocatalytic reaction. The light intensity became the maximum in a few minutes. The reaction temperature was around 288 K. The produced gases were carried with the bubbling flow of CO_2 from the reactor and a portion was periodically sampled to be analyzed by an on-line chromatograph (Shimadzu, GC-8A, TCD, Shincarbon ST, He carrier). In order to find the other products in the liquid phase, a part of the liquid phase was sampled and analyzed by GC-MS (GCMS−Q5050).

3. Results and discussion

3.1. Characterization of photocatalysts

Fig. 1 shows a SEM image of the Ag(3.5)/$CaTiO_3$ photocatalyst before the reaction test. The $CaTiO_3$ particles had a polyhedral crystal shape covered with flat facets. The particle size of the $CaTiO_3$ crystals observed was in the range of 0.2−3 μm. The Ag nanoparticles with the size of 10−120 nm were observed to be deposited preferably on the selected facets. Fig. S1 shows a XRD pattern of the sample, confirming the presence of $CaTiO_3$ crystallites and Ag metal particles. The average crystallites size of the Ag nanoparticles was estimated to be 31.5 nm from the diffraction at 38.1 degree by using Scherrer equation, which consists with the SEM observation. These observations are almost consistent with those in the previous study [22].

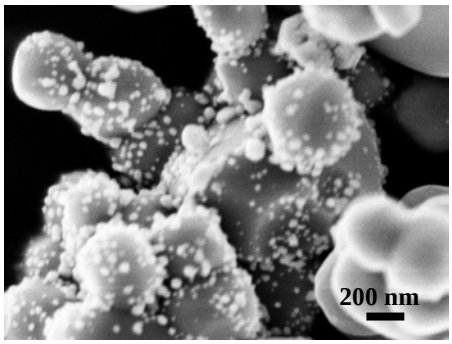

Fig. 1. SEM image of the Ag(3.5)/$CaTiO_3$ sample before use for the photocatalytic reaction test.

3.2. Photocatalytic reduction of CO_2

Fig. 2 shows the time course of the production rates in the photocatalytic CO_2 reduction with water over the Ag(3.5)/$CaTiO_3$ sample in the standard condition with the CO_2 bubbling flow at 288 K. The products were mainly CO and O_2 as well as a small amount of H_2. The production rate of CO and O_2 gradually increased and that of H_2 decreased for initial 6 h. After that, the production rates became constant to be 54 μmol h^{-1} for CO and 25 μmol h^{-1} for O_2, where the former is almost two times higher than the latter. It is noted that the reduction of H^+ to H_2 was very suppressed, i.e., the rate for H_2 production at the initial and the steady state were only 6.3 and 3.1 μmol h^{-1}, respectively, even though the redox potential for H_2 formation (0.0 V, vs. SHE) is obviously higher than that for CO formation (−0.12 V, vs. SHE) [17].

Other gaseous reduction product such as methane was not detected by online TCD-GC. Any other products in the liquid phase, such as methanol, formic acid, and formaldehyde, were not detected by GC-MS. The consumed ratio of the photoexcited electrons and holes was calculated from the production rate of CO, H_2, and O_2 was almost unity (e^-/h^+=1.1) according to the eq. 7, meaning that the products would be almost limited to CO, H_2, and O_2. Based on these facts, the CO selectivity can be calculated as mentioned above (eq. 6). As a result, the reaction selectivity for the CO_2 reduction to CO reached 94% over the Ag(3.5)/$CaTiO_3$ photocatalyst.

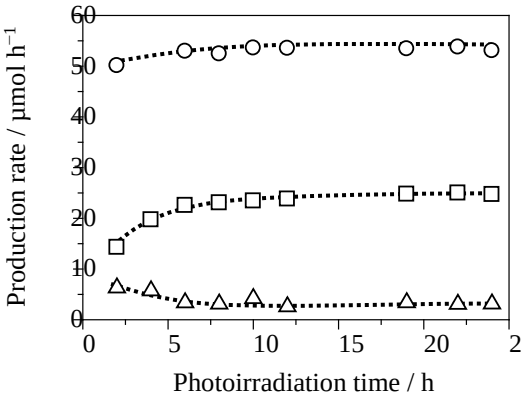

Fig. 2. Time courses of the production rates of CO (circle), H_2 (triangle), and O_2 (square) in the photocatalytic reduction of CO_2 with water over the Ag(3.5)/$CaTiO_3$ sample.

In the present study, the optimum loading amount of Ag was examined and found to be 3.5 wt% as shown in Fig. 3. The photocatalyst without Ag cocatalyst produced H_2 at 6.0 μmol h^{-1} as the main product and the CO very slowly at 2.2 μmol h^{-1}, where the CO selectivity was low such as 26%. This shows that the surface of the bare $CaTiO_3$ photocatalyst would be preferably responsible for the H_2 evolution and the Ag cocatalyst promotes the CO formation. It is suggested that the loading Ag cocatalyst would diminish the active sites for H_2 production on the $CaTiO_3$ surface, and thus increase the high CO selectivity.

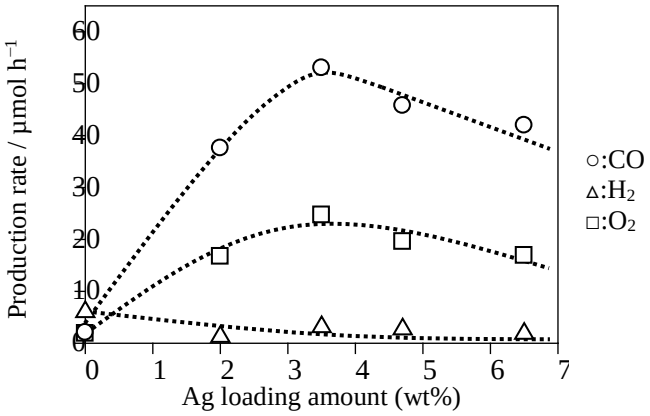

Fig. 3. Production rates of CO (circle), H_2 (triangle), and O_2 (square) over various Ag(*x*)/$CaTiO_3$ photocatalysts with different loading amount of Ag cocatalyst.

The products were not detected without the photocatalyst or without photoirradiation. As mentioned above, the consumed ratio of the photoexcited electrons and holes was consistent (e^-/h^+=1.1). The formation rates for these products became constant and the reaction continuously proceeded for a long time in a steady state. These facts support that this reaction is evidently a photocatalytic reaction. The chemical equations for the predominant reaction can be described as follows: The photocatalytic reduction of CO_2 with photoexcited electrons and protons can form CO and water (eq. 1) and the photocatalytic oxidation of water can produce oxygen and protons (eq. 2). These equations give the total equation of the photocatalytic CO_2 splitting into CO and O_2 (eq. 3), which is a multi-photon process. Although water does not appear in the total equation, it works as an electron source.

Compared with the previous study, many parameters in the reaction condition were changed by changing the reactor as listed in Table S1, such as the amount of catalyst, the light intensity, the irradiation area, the light source giving the light with the specific wavelength distribution, the introducing method of

CO_2 gas, and the reaction temperature. As a result, it is the fact that the production rate of CO was improved as 154 times larger, and also the CO selectivity was improved from 45% to 94%. The selectivity is almost the same level as, or rather slightly higher than, that reported in the electrochemical CO_2 reduction by using a Ag electrode (87%) [24], implying that the high CO selectivity would originate from the property of the Ag cocatalyst. This high selectivity is one of the highest records so far [13,16] and the best value among the heterogeneous photocatalytic CO_2 reduction with water over titanium-based photocatalysts such as Ag-loaded $BaLa_4Ti_4O_{15}$ (69%) [9] and Ag-loaded $La_2Ti_2O_7$ (51%) [11].

The reaction test was additionally performed in the reactor employed in the previous study (reactor A) with the present Ag(3.5)/$CaTiO_3$ sample (Fig. S2). The production rates of CO, H_2 and O_2 were 1.3, 0.65, and 0.98 μmol h^{-1}, respectively, and the CO selectivity was 67%. Both the photocatalytic activity and the selectivity towards CO formation with the reactor A were certainly much less than those with the reactor B. When the same photocatalyst was used, the CO formation rate with the reactor B was 41 times higher than that with the reactor A. This fact evidences that the new reaction condition using the present reactor is essential for the high and selective formation of CO. To discuss the reason for the high conversion, the intensity of light that reached to the photocatalyst was roughly estimated to be 0.05 and 0.10 mW for the previous and current reactor, respectively, which were calculated by multiplying the following three values, the light intensity (22 and 44 mW cm^{-2} at 254 nm in wavelength), the photoirradiation area of the reactor (20 and 155 cm^2), and the relative area of the light emission spectra from each lamp (1.0 and 0.13, in the range of 200–350 nm in wavelength). Thus, it was confirmed that the current reactor provided 2 times larger light intensity than the previous one. It is expected that the production rate of CO would become 2 times larger. In the separate experiment, the reaction test was carried out by using 0.1 g of photocatalyst. The CO production rate was almost the same (49 μmol h^{-1}), meaning that the amount of photocatalyst around 0.1−0.3 g does not influence the production rate so much. Therefore, the difference of the light condition and the catalyst amount cannot explain the high CO formation rate such as 41 times in the present condition, even though the high light intensity would be helpful for the multi-photon reaction to some extent.

Here, it is suggested that another clear factor would be the flow of bubbling CO_2 directly into the liquid phase. Fig. 4 shows the time course of the reaction test when the CO_2 gas was introduced to the reactor without the bubbling. The flow of CO_2 passed through the headspace of the reactor before the reaction for 24 h and also during the photocatalytic reaction. It is obvious that the formation rate of CO was lower than that with the CO_2 bubbling flow even at the initial state, and further it drastically decreased with time. This means that the CO_2 concentration in the aqueous solution would be low at the start of the reaction test and decreased further under photoirradiation. Thus, it is suggested that the bubbling flow is quite efficient for

the dissolution of CO_2 into the aqueous solution. The concentration of CO_2 molecules in the liquid phase should be very important for this photocatalytic reaction. Lower reaction temperature in the present study (Table S1) would also contribute to increase the CO_2 concentration in the solution. To confirm the effect of the concentration of dissolved CO_2 in the solution, the reaction test was carried out at higher temperature (306 K) in the reactor B (Fig. 5). The production rate of H_2 was almost the same as that performed at lower temperature. But the production rate of CO was lower at higher temperature. Therefore, selectivity towards CO formation was lower at higher temperature. This result supports that the higher concentration of dissolved CO_2 provides the higher CO production rate and the higher CO selectivity. In addition, as another possibility, the bubbles might physically facilitate the desorption of gaseous products as small bubbles from the photocatalyst surface.

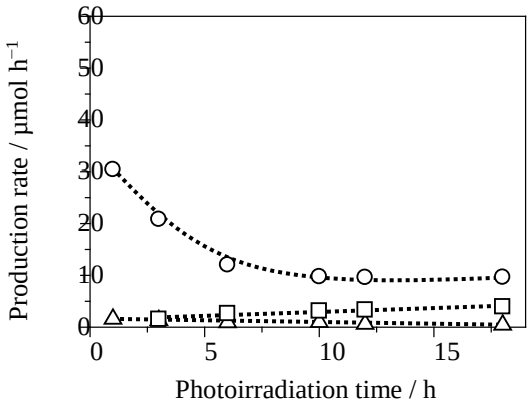

Fig. 4. Time courses of the production rates of CO (circle), H_2 (triangle), and O_2 (square) in the photocatalytic reduction of CO_2 with water over the $Ag(3.5)/CaTiO_3$ sample without the CO_2 bubbling flow.

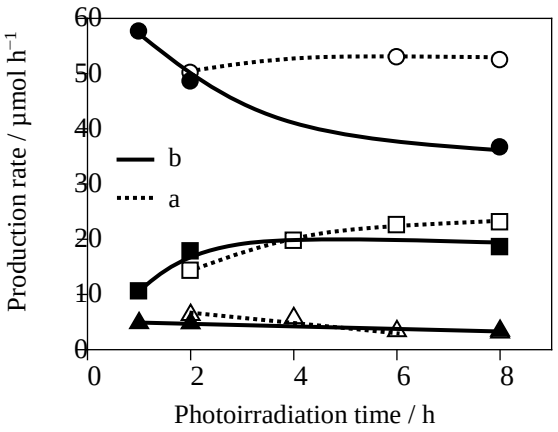

Fig. 5. Time courses of the production rates of CO (circle), H_2 (triangle), and O_2 (square) in the photocatalytic reduction of CO_2 with water over the Ag(3.5)/$CaTiO_3$ sample at 288 K (a) and 306 K (b).

As mentioned above, the product selectivity varied from 89% to 94% with time at the initial period. This implies that the state of the photocatalyst might change as pointed out in the previous study [22]. Fig. 6 shows diffuse reflectance UV−Vis spectra of the Ag(3.5)/$CaTiO_3$ photocatalyst before and after the photocatalytic reaction test, along with that of the pristine $CaTiO_3$ sample. The absorption bands due to the Ag nanoparticles are clearly shown in the range of 350–800 nm in wavelength. Before the reaction, a very broad band with the maximum around 520 nm was observed, which would be derived from the surface plasmon resonance of the Ag nanoparticles. After the reaction, the maximum of the band shifted to 400 nm. These bands depend on silver nanoparticle size [25]. The broad absorption band in fresh catalyst is attributed to the wide particle size distribution, while the relatively narrow absorption band in spent catalyst is attributed to the narrow particle size distribution with smaller particles. As mentioned above, Ag nanoparticles in the fresh Ag(3.5)/$CaTiO_3$ sample was in the size range 10−120 nm estimated from SEM (Fig. 1) and the average crystallites size was 31.5 nm from XRD (Fig. S1). In contrast, Ag nanoparticles in the used sample had relatively narrow size distribution in the range of 20−80 nm after use as shown in the SEM image (Fig. S3), and the average crystallites size was 21.7 nm estimated from XRD (Fig. S4). In addition, Ag loading amount before and after use was almost the same, which was confirmed by XRF analysis. It is suggested that the Ag atoms of the nanoparticles on the oxidative facets are photooxidized to Ag^+ cations and dissolved in the aqueous solution, and the Ag^+ cations are photodeposited on the reductive

facets to form more dispersed Ag nanoparticles. Thus, the Ag nanoparticles responsible for the CO production dispersed via the photooxidation and photodeposition process of the Ag species and diminish the number of the active sites for the H_2 production on the reductive facets of $CaTiO_3$ photocatalyst. From the above reasons, the structural variation of the Ag nanoparticles would increase the production rates of CO slightly and decreased that of H_2 by half at the early stage in Fig. 2.

Here, it is notable that, although the change in the DR UV-Vis spectra was drastic during the reaction test as mentioned above (Fig. 6), the change in the photocatalytic production rates in the time course was not so large (Fig. 2). This means that the Ag species showing the adsorption bands in the visible light region would less contribute to the production rates while the other species would contribute dominantly. In literature, it is proposed that very small Ag nanoclusters exhibiting the absorption band around 350 nm are responsible as the efficient cocatalyst for the photocatalytic reduction of CO_2 [26]. Thus, in the present system, it can be suggested that the dispersed Ag species like as small nanoclusters exhibiting the absorption band in the UV light region are the predominant cocatalyst for CO_2 decomposition.

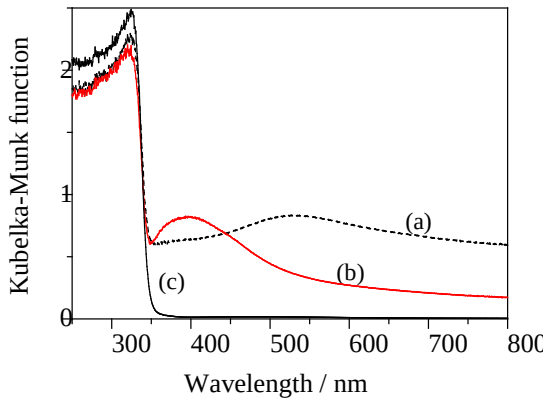

Fig. 6. Diffuse reflectance spectra of the Ag(3.5)/$CaTiO_3$ sample (a) before and (b) after the photocatalytic reaction for CO_2 reduction, and (c) that of the pristine $CaTiO_3$ sample.

On the other hand, the evolution rate of O_2 at the initial stage was not consistent with the production rates of CO and H_2, where the consumed ratio of the photoexcited electrons and holes was apart from unity (e^-/h^+=1.9). The lack of the amount of evolved O_2 was estimated as 46 μmol. Although the reason was not

clarified in this study, oxygen might be photoadsorbed on the surface of photocatalyst as pointed out in the case of TiO_2 [27].

4. Conclusions

In conclusion, in the present study it was revealed that the Ag loaded $CaTiO_3$ crystals is one of the most selective photocatalysts for the photocatalytic CO_2 reduction into CO and O_2 in an aqueous $NaHCO_3$ solution. The selectivity for the CO_2 reduction reached 94%, where the water splitting to produce H_2 was almost suppressed even though the redox potential for H_2 formation is obviously higher than that for the CO formation. It was confirmed that the introducing gaseous CO_2 by a bubbling flow into the reaction solution is quite efficient.

Acknowledgments

This work was financially supported by a Grant-in-Aid for Scientific Research on Innovative Areas “All Nippon Artificial Photosynthesis Project for Living Earth (AnApple)” (No. 25107515) from the Japan Society for the Promotion of Science (JSPS), and the Program for Element Strategy Initiative for Catalysts & Batteries (ESICB), commissioned by the MEXT of Japan. This work was partly carried out by the joint research program of the Artificial Photosynthesis, Osaka City University, Japan.

References

[1] T. Inoue, A. Fujishima, S. Konishi, K. Honda, Nature 277 (1979) 637–638.
[2] M. Halmann, V. Katzir, Sol. Energy Mater. 10 (1984) 85–91.
[3] O. Ishitani, C Inoue, Y. Suzuki, T. Ibusuki, J. Photochem. Photobiol. A 72 (1993) 269–271.
[4] T. J. Meyer, Acc. Chem. Res. 22 (1989) 163–17
[5] H. Inoue, T. Shimada, Y. Kou, Y. Nabetani, D. Masui, S. Takagi, H. Tachibana, ChemSusChem. 4 (2011) 173–179.
[6] N. S. Lewis, D. G. Nocera, Proc. Natl. Acad. Sci. USA 103 (2006) 15729 –15735.
[7] A. Kubacka, M. Fernández-García and G. Colón, Chem. Rev. 103 (2012) 1555–1614.
[8] K. Sayama, H. Arakawa, J. Phys. Chem. 97 (1993) 531–533.
[9] K. Iizuka, T. Wato, Y. Miseki, K. Saito and A. Kudo, J. Am. Chem. Soc. 133 (2011) 20863–20868.
[10] T. Takayama, K. Tanabe, K. Saito, A. Iwase and A. Kudo, Phys. Chem. Chem. Phys. 16 (2014) 24417–24422.
[11] Z. Wang, K. Teramura, S. Hosokawa, T. Tanaka, Appl. Catal. B 163 (2015) 241–247.

[12] S. Iguchi, K. Teramura, S. Hosokawa and T. Tanaka, Catal. Sci. Technol. 6 (2016) 4978–4985.

[13] H. Nakanishi, K. Iizuka, T. Takayama, A. Iwase, A. Kudo, ChemSusChem 10 (2017) 112–118.

[14] Z. Huang, K. Teramura, S. Hosokawa, T. Tanaka, Appl. Catal. B 199 (2016) 272–281.

[15] K. Teramura, Z. Wang, S. Hosokawa, Y. Sakata, T. Tanaka, Chem. Euro. J. 20 (2014) 9906–9909.

[16] Z. Wang, K. Teramura, Z. Huang, S. Hosokawa, Y. Sakata, T. Tanaka, Catal. Sci. Technol. 6 (2016) 1025–1032.

[17] V. P. Indrakanti, J. D. Kubicki, H. H. Schobert, Energy Environ Sci. 2 (2009) 745–758.

[18] H. Mizoguchi, K. Ueda, M. Orita, S.-C. Moon, K. Kajihara, M. Hirano, H. Hosono, Mater. Res. Bull. 37 (2002) 2401–2406.

[19] K. Shimura, H. Yoshida, Energy Environ. Sci. 3 (2010) 615–617.

[20] K. Shimura, H. Miyanaga, H. Yoshida, Stud. Surf. Sci. Catal. 175 (2010) 85–92.

[21] J.S. Jang, P.H. Borse, J.S. Lee, K.T. Lim, O.S. Jung, E.D. Jeong, J.S. Bae, H.G. Kim, Bull. Korean Chem. Soc. 32 (2011) 95–99.

[22] H. Yoshida, L. Zhang, M. Sato, T. Morikawa, T. Kajino, T. Sekito, S. Matsumoto, H. Hirata, Catal. Today 251 (2015) 132–139.

[23] K. Teramura, K. Hori, Y. Terao, Z. Huang, S. Iguchi, Z. Wang, H. Asakura, S. Hosokawa, and T. Tanaka, J. Phys. Chem. C 121 (2017) 8711–8721.

[24] Y. Hori, H.Wakabe, T. Tsukamoto, O. Koga, Electrochem. Acta 39 (1994) 1833–1839.

[25] J. J. Mock, M. Barbic, D.R. Smith, D.A. Schultz, S. Schultz, J. Chem. Phys. 116 (2002) 6755–6759.

[26] M. Yamamoto, T. Yoshida, N. Yamamoto, T. Nomoto, Y. Yamamoto, S. Yagi, H. Yoshida, J. Mater. Chem. A 3 (2015) 16810–16816.

[27] R. I. Bickley, F. S. Stone, J. Catal. 31 (1973) 389–397.